

Thermodynamic and thermochemical investigation of the deposits formed on the cathode surface of aluminum electrolysis cells

François Allard · Gervais Soucy · Loig Rivoaland ·
Martin Désilets

Received: 28 May 2014 / Accepted: 4 November 2014 / Published online: 30 November 2014
© Akadémiai Kiadó, Budapest, Hungary 2014

Abstract The efficiency of the Hall-Héroult process is influenced by the formation of solid or solid-liquid deposits on the cathode block surface. These deposits have a high electrical and thermal resistivity. Hence, they disturb the electrical current path at the aluminum and cathode block interface. The phase diagrams of deposits with a typical composition were calculated by thermodynamic equilibrium, and the results were confirmed by differential scanning calorimetry measurements. The ledge toe is mainly composed by $\text{Na}_3\text{AlF}_6(\text{ss})$, $\text{Al}_2\text{O}_3(\text{s})$, and liquid bath in industrial cells. The liquid fraction in the deposits at temperature lower than 933 °C is due to the presence of $\text{Na}_5\text{Al}_3\text{F}_{14}$, $\text{Na}_2\text{Ca}_3\text{Al}_2\text{F}_{14}$, and NaCaAlF_6 and depends on $[\text{Al}_2\text{O}_3]$, $[\text{CaF}_2]$ and the cryolite ratio (CR). The side ledge in industrial cell contains liquid phase when the CR is lower than 2.8. The sludge contains $\text{Al}_2\text{O}_3(\text{s})$ and liquid bath. The ledge toe grows when the local temperature is lower than the solidification temperature of Na_3AlF_6 .

Keywords Aluminum electrolysis · Thermodynamic · Ledge toe · Sludge · Side ledge · DSC

Introduction

The Hall-Héroult process requires a lot of energy to produce aluminum. The electrical resistivity of various cell components and the heat losses to the surroundings are responsible for the high energy consumption. The heat losses are necessary to maintain the heat balance of the cell and to sustain the protective layer of frozen electrolyte on the sidewall. The formation and behavior of the deposits under the aluminum pad were investigated in order to optimize the efficiency of this process. These deposits cause a restriction on the cathode block surface, thus altering the flow of current, deteriorating the stability of the cells and increasing the cathodic voltage drop [1]. The thermodynamic models of the molten electrolyte used in this process have been significantly improved in the last decade, allowing a better comprehension of the behavior of the deposits [2].

In recent decades, the $\text{NaF-AlF}_3\text{-CaF}_2\text{-Al}_2\text{O}_3$ system with LiF , MgF_2 , and KF additives has been studied by thermal analysis (TA) and differential thermal analysis (DTA) in order to find the liquidus temperature of the electrolytic bath when undersaturated in alumina [3–7]. The solubility of alumina in molten salts was determined by measuring the mass losses of an alumina disk in a cryolitic bath [8]. These studies determined the liquidus temperature of various melt compositions and described the behavior of the bath at high temperatures. However, according to thermal modeling results [1], the temperature inside the ledge toe and bottom freeze can be lower than the temperature of crystallization of the cryolite. Recently, a thermodynamic study was applied to describe the molten cryolite system in a typical industrial electrolysis cell in order to optimize the composition of the electrolytic bath [9].

F. Allard · G. Soucy (✉) · M. Désilets
Department of Chemical Engineering and Biotechnological
Engineering, Université de Sherbrooke, C1 - Pavillon J. Armand
Bombardier, 2500 Boulevard de l'Université, Sherbrooke,
QC J1K 2R1, Canada
e-mail: Gervais.Soucy@USherbrooke.ca

L. Rivoaland
Rio Tinto Alcan (Arvida Research and Development Centre),
1955 Boulevard Mellon, Jonquière, QC G7S 4K8, Canada

The chemical composition of the deposits on the cathode surface varies depending on the location where the sample is collected. According to Allard et al. [10], the ledge toe area close to the sidewall has a chemical composition close to the bath above the metal. The ledge toe area farther from the sidewall is supersaturated in alumina and has a higher cryolite ratio (CR). The CR is the molar ratio of NaF/AlF₃ calculated from the phases detected by XRD (X-ray diffraction). Moreover, the ledge toe can have a composition similar to the bottom crust (up to 85 % of Al₂O₃). Typically, the bottom crust has a mass fraction of alumina between 65 and 85 % and a much lower concentration of AlF₃ and CaF₂ than the electrolytic bath [11]. Sludge located under the aluminum pad has a typical alumina concentration between 20 and 50 %, a CaF₂ concentration of 3 % (diluted by the high concentration of alumina), and a higher CR than the bath [10–13]. Thick samples of sludge can be located between the ledge toe and the center of the electrolysis cell. A thin film of bath supersaturated in alumina can cover a large part of the cathode surface and it has a similar composition when compared to the sludge. Freezing of bath can occur if the CR is high (low superheat of the bath) or if there are excessive heat losses from the bottom of the cell. The bottom freeze is a deposit which contains a low concentration of alumina. It can be located at the same position than the sludge. Figure 1 shows the locations of the deposits in industrial electrolysis cell.

The side ledge is formed on the sidewall by the primary crystallization of the cryolite (Na₃AlF₆) [14]. The side ledge formed at equilibrium conditions has a composition close to pure Na₃AlF₆. The liquid phase surrounding the Na₃AlF₆ will be more concentrated in AlF₃, CaF₂, and Al₂O₃ and will diffuse toward the bath [15]. However, the rate of cooling may be sufficiently high to favor dendritic crystal growth. Depending on the cooling rate, the liquid phase can be “trapped” into the dendrites during the formation of the side ledge, especially if there is supercooling [15, 16]. Thus, the side ledge has a heterogeneous

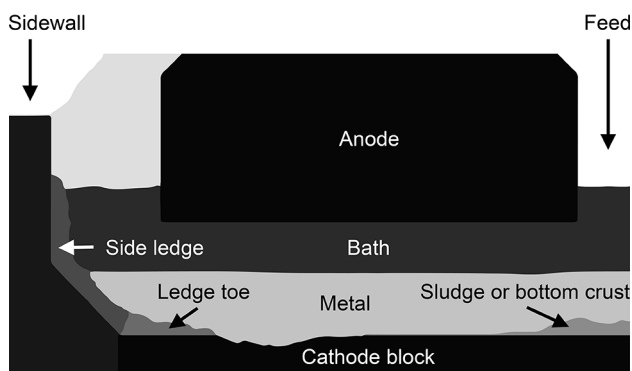


Fig. 1 Diagram of the deposits in industrial electrolysis cell

composition which depends on the bath chemistry and rate of cooling.

In this article, a thermodynamic study will be used to determine the temperature of transition of the different phases in the deposits that form on the cathode surface. The phase diagrams were validated by differential scanning calorimetry (DSC) in order to ensure the relevance of the results obtained by the thermodynamic calculations. Thermogravimetry and differential thermal analysis (TG/DTA) were conducted in order to verify the mass losses and energies involved during the experiments. The thermodynamic study will help in understanding the behavior of the deposits at operating conditions based on their typical chemical composition.

Experimental methods

Sample preparation

The thermal analyses were completed in order to assess the reactions occurring in the deposits during the operation of an electrolysis cell and to validate the thermodynamic data. Chemical products with high purity were used as reactants. The following chemical products: Na₃AlF₆ (99.9 %), NaF (99 %), and α-Al₂O₃ (99.95 %) were sourced from Alfa Aesar; AlF₃ (99.9 %) and CaF₂ (99.9 %) were obtained from Sigma-Aldrich. The melting point of the Na₃AlF₆ was found to be at 1,010 °C based on a DSC analysis. Moreover, its composition was validated by XRD analysis.

The chemical compositions of typical deposits were reproduced in the samples. Each reactant was ground into a fine powder of similar particle size and mixed together prior to the thermal analysis. The variables in this study were the CR and the equivalent quantity of CaF₂ in the bath without considering the alumina concentration. The total quantity of AlF₃ and CaF₂ was diluted with alumina for samples with high alumina concentrations. Equation 1 was used to calculate the concentration of CaF₂ in the samples analyzed by the DSC and by the thermodynamic equilibrium:

$$w_{\text{CaF}_{2\text{eq}}} = \frac{w_{\text{CaF}_2}}{1 - w_{\text{Al}_2\text{O}_3}}. \quad (1)$$

Methods

Differential scanning calorimetry (DSC)

Most of the reactions were conducted in a Netzsch DSC 404 F3 Pegasus in order to evaluate the temperature of phase transition. The DSC equipped with a platinum measuring head can reach a temperature of 1,500 °C. The samples analyzed in this study were heated from 20 to

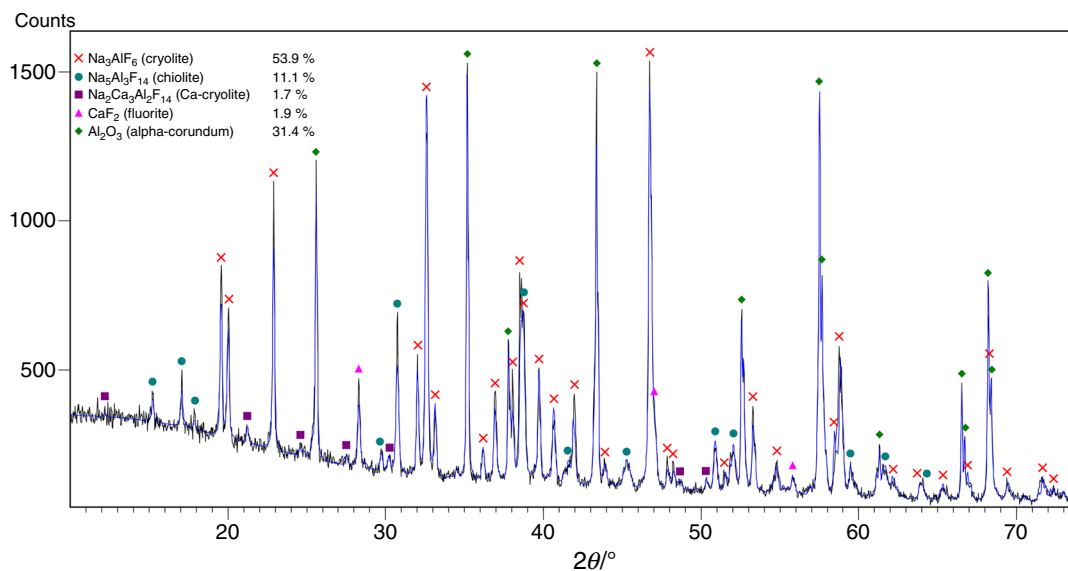


Fig. 2 Rietveld refinement processed on XRD data of a ledge toe sample

1,050 °C, cooled from 1,050 to 400 °C and heated a second time to 1,050 °C at a rate of 10 °C min⁻¹. The controlled atmosphere of each test was assured by a continuous flow of nitrogen. The reactants were put in a graphite crucible of 85 μL (Netzsch), and a graphite cover was installed on the crucible before measurements. The graphite cover has a small vent hole in the center. Therefore, pressure build-up cannot occur inside the crucible. The cover helps in obtaining a better base line, to lower the evaporation and to achieve a better repeatability. Typically, 35 mg of fresh reactant was added before each DSC analysis.

Thermogravimetry and differential thermal analysis (TG/DTA)

Some reactions were repeated to evaluate the mass losses during the analysis. These tests were performed by using a Setaram Setsys 2400. The measuring head installed in this instrument is able to reach a temperature of 1,600 °C. The heating rates were controlled to 10 °C min⁻¹. The reaction chamber was filled with argon as to reduce oxidation. A crucible (platinum/rhodium 10 %) without a cover was used. Typically, 20 mg of reactant was put in the crucible before each test.

X-ray diffraction (XRD)

Some samples were analyzed by XRD in order to obtain their chemical composition. The samples were ground prior to the analysis. XRD characterization was completed with a PANalytical X'Pert PRO MPD diffractometer. The data were collected with a PIXcel^{1D} detector. The rotation speed

of the sample holder was set to 1 s⁻¹. The diffraction pattern was gathered from 10 to 74° at a 2θ angle with the Cu Kα radiation. The chemical compositions of the samples discussed in this article were obtained with a Rietveld method performed on XRD results. XRD analyses of deposits lead to the detection of the following compounds: Na₃AlF₆, Na₅Al₃F₁₄, NaAlF₄, Na₂Ca₃Al₂F₁₄, NaCaAlF₆, Na₄Ca₄Al₇F₃₃, CaF₂, NaF, AlF₃, α-Al₂O₃, γ-Al₂O₃, δ-Al₂O₃, θ-Al₂O₃, β-Al₂O₃, Al₄C₃, Al, and C. The Rietveld refinements were obtained with the software PANalytical HighScore Plus. Figure 2 provides an example of the Rietveld refinement processed on XRD data from a sample of ledge toe. Only the main phases were selected in this example. The Rietveld refinement (blue line) was added over the XRD pattern (black line).

Theoretical calculations

Thermodynamic equilibrium

The formation of deposits at the cathode surface was investigated by a thermodynamic equilibrium analysis in order to assess the behavior of deposits in industrial operating conditions. Thermodynamic equilibrium calculations were achieved by using the FactSage software version 6.4. This software calculates the thermodynamic equilibrium based on the Gibbs free energy minimization [2]. The FTHall database was selected to model the NaF–AlF₃–CaF₂–Al₂O₃ system. The calculations were all carried out at atmospheric pressure. All concentrations presented in this article are expressed in mass fraction (%) and

they are expressed with brackets. The following solutions were selected in the FTHall database: bath (NaF, CaF₂, AlF₃, Al₂F₆, Na₂O, CaO, and Al₂O₃), low temperature cryolite (Na₃AlF₆, AlF₆, Ca₃AlF₆), high temperature cryolite (Na₃AlF₆, Na₃AlF₄, AlF₄, AlF₆, Ca₃AlF₆, Ca₃AlF₄), and metal (Al, Na, Ca). These solid species were selected: Na, Na₂O, NaF, Al, Al₂O₃, AlF₃, NaAlO₂, NaAl₉O₁₄, Na₂Al₁₂O₁₉, Na₃AlF₆, Na₅Al₃F₁₄, Ca, CaO, CaF₂, CaAl₂O₄, CaAl₄O₇, CaAl₁₂O₁₉, Ca₃Al₂O₆, CaAlF₅, Ca₂AlF₇, Ca₁₂Al₁₄F₂O₃₂, NaCaAlF₆, NaCaAl₂F₉, Na₂Ca₃Al₂F₁₄, and Na₄Ca₄Al₇F₃₃. The gas species which came from the FTHall and FactPS database were also selected. The phase diagrams calculated with FactSage were confirmed by DSC analysis with the heating and cooling curves.

Reactants used to reproduce the industrial deposits

The chemical composition of the products synthesized by the reactions between Na₃AlF₆, CaF₂, and AlF₃ were validated by XRD analysis. First of all, the reactants were mixed together and placed in a graphite crucible. The crucible was placed in a furnace in order to perform the reaction under nitrogen atmosphere. A thermocouple was placed in the crucible in order to confirm the temperature. After the heating and cooling steps, the reactants produced the following compounds: Na₅Al₃F₁₄, Na₂Ca₃Al₂F₁₄, NaCaAlF₆, and Na₄Ca₄Al₇F₃₃; in addition Na₃AlF₆, AlF₃, and CaF₂ remained unreacted. Furthermore, a thermodynamic equilibrium analysis with the Na₃AlF₆, CaF₂, AlF₃, and Al₂O₃ system confirmed the production of the previous compounds. Thus, the industrial deposits will be represented using Na₃AlF₆, CaF₂, AlF₃, and Al₂O₃ as reactants in the thermochemical investigation.

Chemical composition of industrial deposits

Table 1 shows the typical concentration of the different deposits that form on the cathode surface of an aluminum electrolysis cell. The main compounds found by XRD and Rietveld analysis in the deposits were Na₃AlF₆, Na₅Al₃F₁₄, Na₂Ca₃Al₂F₁₄, and α-Al₂O₃ according to previous work [17]. The chemical composition indicated in Table 1 is limited to Na₃AlF₆, AlF₃, CaF₂, and Al₂O₃ in order to simplify the presentation. It is also important to note that some industrial electrolysis cells may have an AlF₃ and CaF₂ content higher or lower than these data, depending on the operating conditions. The composition of the reactant used in the thermodynamic equilibrium analysis and the DSC tests will be based on the results of Table 1.

The general composition of the deposits varies a lot as a result of the local parameters (surrounding composition, temperature, and rate of cooling) in the cell which impact

Table 1 General mass composition of the various deposits in the Hall-Héroult process [10–14]

Type of deposits	AlF ₃ / %	CaF ₂ / %	Al ₂ O ₃ / %	Na ₃ AlF ₆ /%
Side ledge	1–13	1–6	1–5	
Ledge toe with low [Al ₂ O ₃]	5–13	4–6	2–10	
Ledge toe with high [Al ₂ O ₃]	2–13	2–5	10–85	100–w _{AlF₃}
Bottom freeze	2–13	4–6	2–10	–w _{CaF₂} –w _{Al₂O₃}
Sludge	2–10	2–5	20–50	
Bottom crust	2–5	2	65–85	

the formation mechanisms. The side ledge formed at equilibrium has a composition close to pure Na₃AlF_{6(ss)}. However, previous observations showed a side ledge with a composition near to the bath (CR between 2.2 and 2.5) [10, 17]. Generally, the side ledge is more neutral and had a lower [CaF₂], [AlF₃], and [Al₂O₃] than the bulk bath [14].

Results and discussion

Reactions in the NaF–AlF₃–CaF₂–Al₂O₃ system

The composition of the deposits on the cathode surface can be described by the NaF–AlF₃–CaF₂–Al₂O₃ system. Al₂O₃ interacts with the NaF–AlF₃–CaF₂ system principally by modifying the liquidus temperature. The Al₂O₃ content decreases the solidification temperature of the cryolite solution in alumina undersaturated bath, while this temperature remains constant in supersaturated bath. As it is locally added, Al₂O₃ is in supersaturation condition. Part of the Al₂O₃ remains undissolved and sinks into the bath to form sludge. A very high temperature is required in order to completely melt the sludge at the bottom of the cell because of its high liquidus temperature. There is an important temperature gradient inside the side ledge and the ledge toe, due to important heat losses by the sidewall and by the bottom of the electrolysis cell. Thus, the reactions occurring in the deposits are complex and evolve at a wide range of temperatures. Table 2 shows the main reactions that occur in the deposits during the operation of an industrial electrolysis cells. The temperatures of the reactions were obtained by thermodynamic calculations.

The letter *L* represents the liquid electrolytic bath in the system. The liquid solution is mainly composed of NaF, AlF₃, Na₂O, Al₂O₃, CaF₂, and CaO according to thermodynamic calculations. The composition of the main crystalline phases is based on previous work [17]. Accordingly, the main phases in the deposits taken in industrial cells are Na₃AlF₆, Na₅Al₃F₁₄, Na₂Ca₃Al₂F₁₄, and α-Al₂O₃. These

Table 2 Main reactions in the NaF–AlF₃–CaF₂ system according to thermodynamic calculations

$\alpha - \text{Na}_3\text{AlF}_6(\text{s}) \rightarrow \beta - \text{Na}_3\text{AlF}_6(\text{s})$	563 °C
$\beta - \text{Na}_3\text{AlF}_6(\text{s}) \rightarrow \text{L}$	1,009 °C
$\text{Na}_5\text{Al}_3\text{F}_{14}(\text{s}) \rightarrow \text{L} + \text{Na}_3\text{AlF}_6(\text{s})$	726 °C
$\text{Na}_5\text{Al}_3\text{F}_{14}(\text{s}) \rightarrow \text{L}$	873 °C
$\text{Na}_5\text{Al}_3\text{F}_{14}(\text{s}) + \text{AlF}_3(\text{s}) \rightarrow \text{L} + \text{Na}_5\text{Al}_3\text{F}_{14}(\text{s})$	685 °C
$\text{Na}_2\text{Ca}_3\text{Al}_2\text{F}_{14}(\text{s}) \rightarrow \text{L} + \text{CaF}_2(\text{s})$	754 °C
$\text{Na}_2\text{Ca}_3\text{Al}_2\text{F}_{14}(\text{s}) \rightarrow \text{L}$	1,031 °C
$\beta - \text{NaCaAlF}_6(\text{s}) \rightarrow \alpha - \text{NaCaAlF}_6(\text{s})$	654 °C
$\alpha - \text{NaCaAlF}_6(\text{s}) \rightarrow \text{L} + \text{Na}_2\text{Ca}_3\text{Al}_2\text{F}_{14}(\text{s})$	710 °C
$\alpha - \text{NaCaAlF}_6(\text{s}) \rightarrow \text{L}$	931 °C

compounds were detected by XRD. The reactions will be described with the phase diagrams (Figs. 5, 6, 7).

DSC investigation in the formation of deposits

Analysis of synthetic bath

The reactions that occur during the process were investigated with a DSC method. The reactants (Na₃AlF₆, AlF₃, CaF₂, and α -Al₂O₃) were placed in a graphite crucible with a cover. The peak temperatures of each reaction observed in the DSC measurements were used to determine the phase transitions. Such an approach usually overestimates the temperature of phase transition because of the constant heating rate (10 °C min⁻¹) delivered by the furnace and the time needed for the reaction [18, 19]. As expected, a similar analysis done during the cooling step will underestimate the temperature for the same reason. The heat transfer between the source and the sample is not instantaneous and depends on the conduction, convection, and radiation inside the apparatus [19, 20]. These phenomena introduce a “thermal lag” which delays the peak in the DSC or DTA curve [20]. A higher heating rate increases the “thermal lag” [19]. The heating rate and cooling rate of 10 °C min⁻¹ are a compromise between duration of data acquisition and proper results. The temperature calculated by thermodynamic equilibrium will therefore be between the temperatures determined during the heating and cooling steps. Each sample was heated a second time in order to evaluate the effect of the irreversible reactions on the peak temperatures found by DSC. Figure 3 illustrates the difference between the first heating and second heating steps on the transition of α -Na₃AlF₆ to β -Na₃AlF₆ for a sample with a CR of 2.2, [CaF_{2eq}] of 5 % and [Al₂O₃] of 10 %.

The temperatures of 564 and 528 °C were determined from DSC measurements in the first and second heating steps, respectively. The first heating of the synthetic bath shows a similar conversion of α -Na₃AlF₆ to β -Na₃AlF₆

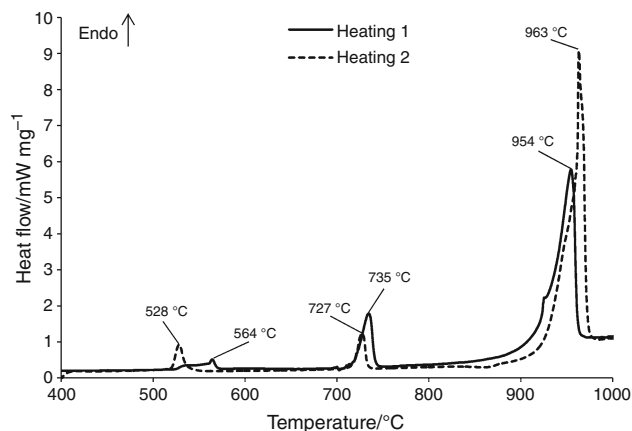


Fig. 3 Typical DSC curves of synthetic bath (CR = 2.2, CaF_{2eq} = 5 % and Al₂O₃ = 10 %)

than pure Na₃AlF₆ (563 °C according to thermodynamic calculations). This temperature of conversion decreased when NaCaAlF₆ is dissolved in the Na₃AlF_{6(ss)}. The transition α -Na₃AlF₆ to β -Na₃AlF₆ occurs at 526 °C according to thermodynamic calculations made with the same bath chemistry. The second heating showed the conversion of α -Na₃AlF₆ to β -Na₃AlF₆ when NaCaAlF₆ is partially dissolved (528 °C). The second heating of the sample helped to accurately determine the temperature of transition of α -Na₃AlF₆ to β -Na₃AlF₆ in the NaF–AlF₃–CaF₂–Al₂O₃ system compared to thermodynamic equilibrium.

A DSC measurement was completed with pure cryolite. It showed a peak temperature at 567 °C corresponding to the α -Na₃AlF₆ to β -Na₃AlF₆ transition. Thermodynamic calculation shows this reaction at 563 °C with pure cryolite. Thus, CaF₂ content decreased the temperature of transition of α -Na₃AlF₆ to β -Na₃AlF₆.

The bath began to melt at a temperature close to the second endothermic peak. This temperature was 735 °C for the first heating step and 727 °C for the second. The Na₃AlF₆ solid solution melted completely at 954 and 963 °C in the first and second heating steps, respectively. The melting temperature varied depending on the chemical composition, as indicated by the results of the additional DSC investigations found in Figs. 5–7. They were integrated into the phase diagrams calculated by thermodynamic equilibrium.

DSC analysis of industrial bath

A sample of industrial bath, with increased [Al₂O₃], was also analyzed by DSC (Fig. 4). The chemical composition of this typical industrial bath was 11 % AlF₃, 5 % CaF_{2eq}, and 10 % Al₂O₃ (CR of 2.2) as determined by XRD. The transition of α -Na₃AlF₆ to β -Na₃AlF₆ occurred at 524 °C according to the first heating of the sample and at 521 °C

within the second heating. These transition temperatures found by the first and second heating occurred at closer temperatures with the industrial bath than synthetic bath. The difference between the results of industrial bath and synthetic bath occurred because the industrial bath had already been heated. Moreover, the industrial bath showed also endothermic peak at 720 and 938 °C according to the first heating.

Thermodynamic phase diagrams of the deposits in the Hall-Héroult process

The thermodynamic investigation aims to describe the behavior of the deposits in real industrial operating

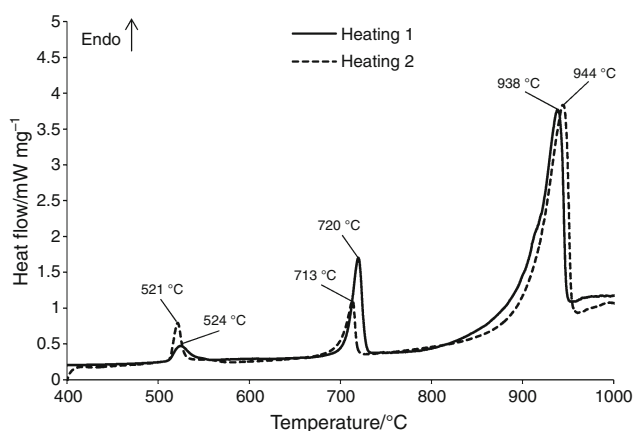


Fig. 4 DSC curves of industrial bath (CR = 2.2, $\text{CaF}_{2\text{eq}} = 5\%$ and $\text{Al}_2\text{O}_3 = 10\%$)

conditions. Figures 5–7 show the reactions that occur in the deposits based on the composition described in Table 1. The phase diagrams were calculated at thermodynamic equilibrium with FactSage V. 6.4. The peak temperatures found by DSC are indicated by data points in each phase diagram (Figs. 5–7). The endothermic reactions are presented by black shapes (heating step). The exothermic reactions are expressed by empty shapes (cooling step). The black triangles show the transition temperatures of $\alpha\text{-Na}_3\text{AlF}_6$ to $\beta\text{-Na}_3\text{AlF}_6$ and these temperatures come from the second heating step. All other black-filled shapes display the data determined with the first heating step. The temperatures when the melting process begun are indicated by diamonds, or circles in highly acidic bath, and the melting temperatures of $\text{Na}_3\text{AlF}_{6(\text{ss})}$ are indicated by squares.

Phase diagram of Al_2O_3

The first phase diagram is related to the alumina mass fraction in electrolytic bath (Fig. 5). It shows the reactions in an acid bath (CR of 2.2) with a typical $[\text{CaF}_{2\text{eq}}]$ of 5%. The ledge toe typically contains a $[\text{CaF}_{2\text{eq}}]$ around 5% and is undersaturated in Al_2O_3 at a location close to the sidewall and supersaturated further from the sidewall [17]. The sludge is highly supersaturated in Al_2O_3 ($[\text{Al}_2\text{O}_3]$ of 20 to 80%) [12, 13]. The melting temperature of the $\text{Na}_3\text{AlF}_{6(\text{ss})}$ impacts the formation and melting of the ledge toe and side ledge. The $\text{Na}_3\text{AlF}_{6(\text{ss})}$ is a solid solution with dissolved CaF_2 and AlF_3 . This solid solution is stable from 525 to

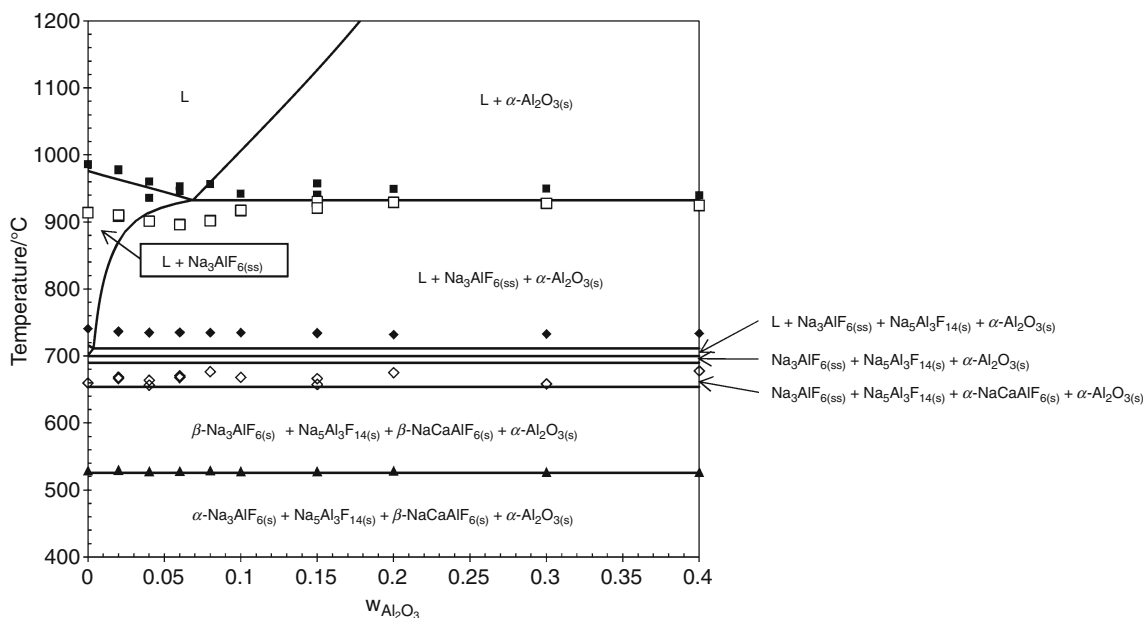


Fig. 5 Phase diagram of the Al_2O_3 mass fraction in a bath of CR = 2.2 and $\text{CaF}_{2\text{eq}} = 5\%$

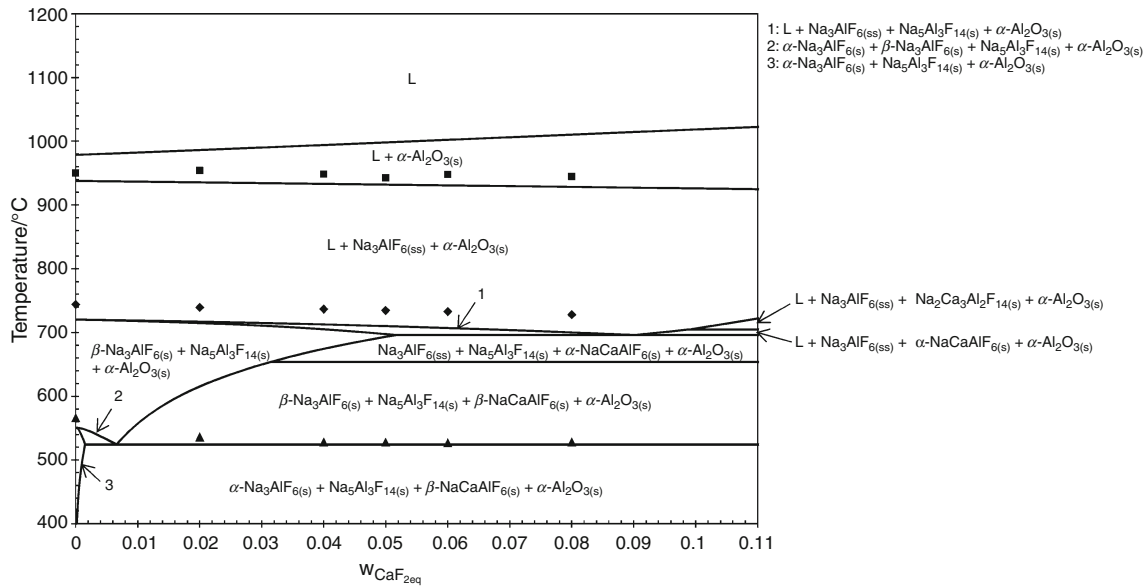


Fig. 6 Phase diagram of the CaF_{2eq} content in a bath of CR = 2.2 and $Al_2O_3 = 10\%$

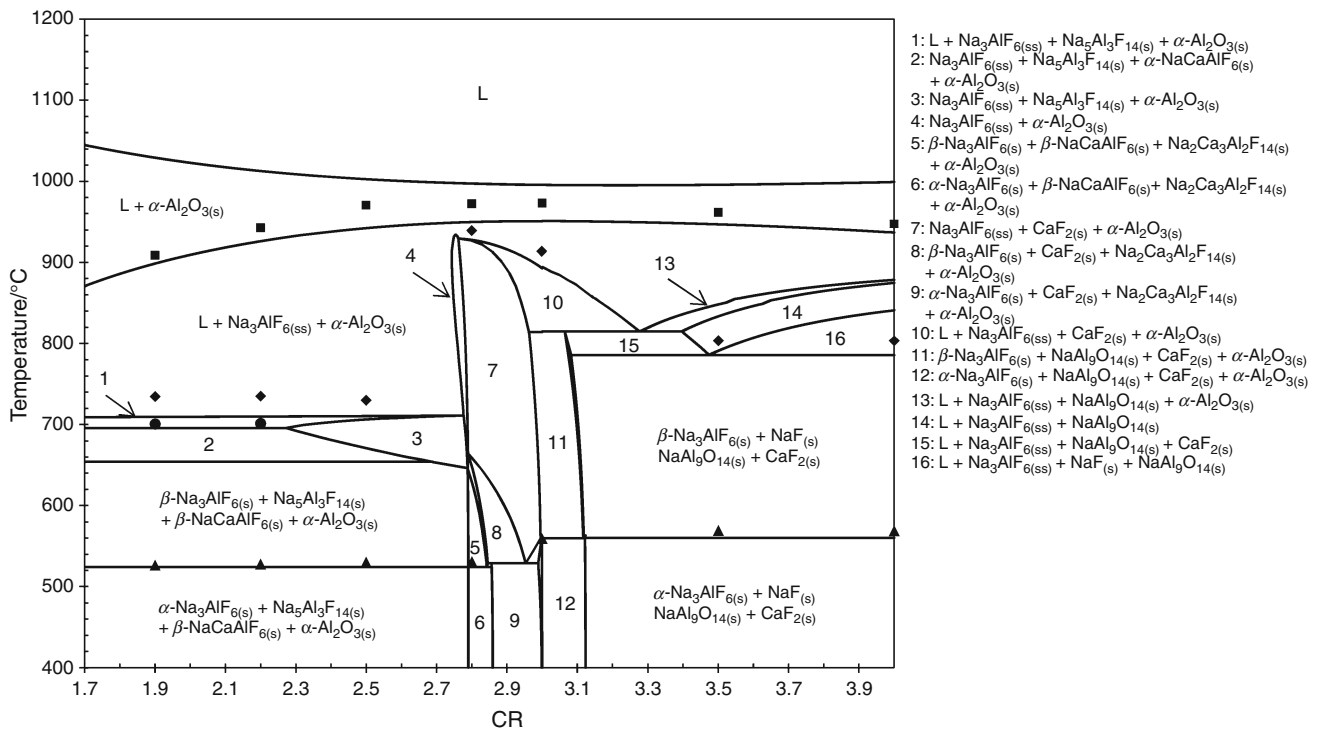


Fig. 7 Phase diagram of the cryolite ratio in a bath of $CaF_{2eq} = 5\%$ and $Al_2O_3 = 10\%$

933 °C (melting temperature of $Na_3AlF_6(ss)$) according to thermodynamic equilibrium calculations.

According to the thermodynamic equilibrium, the reaction of $\alpha-Na_3AlF_6$ to $\beta-Na_3AlF_6$ occurs at 526 °C. The DSC results showed an average transition temperature of 529 ± 1 °C. When the bath is undersaturated ($[Al_2O_3] < 8\%$ at 960 °C), the melting temperature of

$Na_3AlF_6(ss)$ is highly influenced by the Al_2O_3 concentration. This transition occurs at a constant temperature of 933 °C in supersaturated bath. The DSC curves showed an endothermic peak around this transition temperature, and the average temperature was 947 ± 7 °C according to the peak detected during the first heating step. The heating and the cooling steps were located over and under the

temperature determined by thermodynamic equilibrium. $\text{Na}_5\text{Al}_3\text{F}_{14}$ is the first compound that melts in this system. The melting of this compound begins at 698 °C and it ends at 711 °C according to thermodynamic calculations. The melting temperature of $\text{Na}_5\text{Al}_3\text{F}_{14}$ is depressed by the alumina concentration up to saturation ($[\text{Al}_2\text{O}_3] < 0.4 \%$ at 711 °C). The melting of $\text{Na}_5\text{Al}_3\text{F}_{14}$ occurs at 716 °C without Al_2O_3 , and with 5 % $\text{CaF}_{2\text{eq}}$. The melting of the solid solution mostly composed by Na_3AlF_6 proceeds continuously between 711 and 933 °C in supersaturated bath. The liquidus temperature of the bath increased quickly when the $[\text{Al}_2\text{O}_3]$ is higher than 7 %.

Phase diagram of $\text{CaF}_{2\text{eq}}$

The deposits typically have a $[\text{CaF}_{2\text{eq}}]$ between 4 and 7 % according to previous study [17]. The concentration may fluctuate depending on the specific operating condition and Ca concentration in the feed. According to thermodynamic analysis, $\beta\text{-NaCaAlF}_6$ is stable at room temperature. However, only a small quantity of this compound was detected in the deposits analyzed by XRD [17]. Most of the calcium detected came from the compound $\text{Na}_2\text{Ca}_3\text{Al}_2\text{F}_{14}$. NaCaAlF_6 has a low crystallinity and cannot be entirely determined by XRD [21]. A Pot Flux Channel detector must be used to analyze the total content of calcium [22]. The residual calcium can be attributed to NaCaAlF_6 . NaCaAlF_6 forms a solution with $\alpha\text{-Na}_3\text{AlF}_6$ and $\beta\text{-Na}_3\text{AlF}_6$ in solid phase. A low $[\text{NaCaAlF}_6]$ is dissolved in $\alpha\text{-Na}_3\text{AlF}_6$. The fraction of NaCaAlF_6 dissolved in α or $\beta\text{-Na}_3\text{AlF}_6$ increased with temperature [23]. The maximum solubility of the NaCaAlF_6 is reached at 700 °C according to equilibrium calculations of the phases reported in the diagram presented previously (Fig. 5). This temperature corresponds to the beginning of the liquid bath formation. A fraction of the calcium will be found in the liquid bath at higher temperature. Figure 6 depicts the reactions in the bath when the $[\text{CaF}_{2\text{eq}}]$ varies.

The calcium content decreased the temperature of the first endothermic peak in the second heating step. The first endothermic peak corresponds to the transformation of $\alpha\text{-Na}_3\text{AlF}_6$ to $\beta\text{-Na}_3\text{AlF}_6$. This peak was detected at 567 ± 1 °C without CaF_2 and it occurred at an average of 528 ± 1 °C when the $[\text{CaF}_{2\text{eq}}]$ was higher than 4 %. The $\text{CaF}_{2\text{eq}}$ was used in order to neglect the dilution of the alumina and to offer a better representation of the behavior in the deposits supersaturated in alumina. The reaction of $\beta\text{-NaCaAlF}_6$ to $\alpha\text{-NaCaAlF}_6$ occurs at 654 °C according to thermodynamic equilibrium. The bath begins to melt at 720 °C without CaF_2 and this temperature decreases with increasing $[\text{CaF}_2]$. Furthermore, the temperature of the second endothermic peak decreased with $[\text{CaF}_{2\text{eq}}]$ between 0 and 8 %. The bath begins to melt at 698 °C with a $[\text{CaF}_{2\text{eq}}]$ of 5 %.

$\text{Na}_3\text{AlF}_{6(\text{ss})}$ finishes to melt at 950 °C without CaF_2 and at 925 °C with 11 % of $\text{CaF}_{2\text{eq}}$ in the bath. The dissolution of Al_2O_3 in the bath decreases when the $[\text{CaF}_2]$ increases. Thus, a high content of CaF_2 in the liquid is detrimental to the dissolution of the sludge. On the other hand, a high $[\text{CaF}_2]$ can help in reducing the formation of freeze and ledge toe on the cathode surface due to a lower melting temperature. However, a bath highly concentrated in CaF_2 will also affect the formation of the side ledge close to the bath because of its lower melting temperature. $\text{Na}_2\text{Ca}_3\text{Al}_2\text{F}_{14}$ appears in the phase diagram at $[\text{CaF}_{2\text{eq}}]$ higher than 10 %. $\text{Na}_4\text{Ca}_4\text{Al}_7\text{F}_{33}$ forms with high acidity content but it was not detected by XRD in previous work.

Phase diagram of NaF/AlF_3

The chemistry of the bath changes during the operation of an electrolysis cell due to various operating conditions and events (bath evaporation, anode crust losses, siphoning of bath, chemical composition adjustments, etc.). Previous work showed that highly supersaturated deposits had a higher CR than the bath above the metal [10]. Furthermore, migration of sodium ions toward the cathode is responsible for a higher concentration of sodium near the surface of the cathode block. Thus, the CR of the ledge toe and the sludge are higher than the CR of electrolysis bath and it varies between 2.4 and 2.8 [12, 13, 17]. The extremity of the ledge toe, far from the sidewall, and the sludge are supersaturated in Al_2O_3 . Their behavior can be described by a phase diagram with $[\text{Al}_2\text{O}_3]$ higher than the saturation point. The phase diagram in Fig. 7 shows the impact of the CR on the reactions that occur in the electrolytic bath.

As confirmed by DSC and thermodynamic equilibrium calculations, the CR had a major impact on the transformation temperature of $\text{Na}_3\text{AlF}_{6(\text{ss})}$ into liquid bath. The melting of this solution occurs at higher temperature with a neutral CR and it decreases with increasing or decreasing CR. At CR = 3.0 the melting of $\text{Na}_3\text{AlF}_{6(\text{ss})}$ occurs at 951 °C. It becomes 910 °C at CR = 2.0 and 937 °C at CR = 4.0. The formation of the liquid solution begins at lower temperature with an acid bath (698 °C with CR < 2.3 and 711 °C with CR around 2.7) than with basic bath (786 °C). The concentration of acid compounds, $\text{Na}_5\text{Al}_3\text{F}_{14}$ and $\text{Na}_2\text{Ca}_3\text{Al}_2\text{F}_{14}$, is low at CR = 2.8 and it is zero at CR = 3.0. Thus, the DSC analysis did not detect an endothermic peak at temperature around 700 °C for CR of 2.8 and 3.0.

The bath begins to melt at 918 °C with a CR of 2.8 according to thermodynamic calculations. The DSC analysis showed a small peak at 939 °C, thus confirming the result of the thermodynamic calculations at CR = 2.8. The sample of CR = 3.0 showed a small endothermic peak at 911 °C despite a less acidic CR. The thermodynamic

equilibrium also showed a similar transition at 894 °C. According to thermodynamic calculations, the melting of bath with CR = 3.0 begins at 814 °C due to the CaF₂ content. The Na₃AlF₆–CaF₂ system was studied by Holm in 1968 [24]. He reported a solidus for this system at around 785 °C within the cooling curve (0.5–1 °C min⁻¹). However, a small evaporation may have displaced the NaF/AlF₃ ratio by the loss of NaAlF₄ during the experiments made by Holm. Also, the addition of CaF₂ can modify the acidity of the bath and depress the eutectic temperature of this binary system [24]. The DSC experiment of the sample with CR = 3.0 only showed peaks at 544, 886, and 895 °C with the cooling step and no peak was detected around 785 °C. The cover used in the DSC experiments and faster heating and cooling step (10 °C min⁻¹) should have limited the evaporation.

The risk of formation of excessive ledge toe is higher if its chemistry comes closer to the neutral point. The expansion of the ledge toe considerably reduces the contact surface between the aluminum and the cathode block. Furthermore a neutral bath leads to the formation of CaF_{2(s)} which will sink toward the cathode block. There is formation of NaF_(s), CaF_{2(s)}, and β-Al₂O_{3(s)} when the NaF/AlF₃ ratio is higher than 3.0.

Liquid fraction in the deposits

The liquid fraction in the deposits was determined by thermodynamic calculations. The melting of an acid bath begins around 700 °C depending on the CaF₂, AlF₃, and Al₂O₃ content. This mixture completely melts at approximately 940 °C, without considering the Al₂O₃ dissolution in supersaturated bath (exact temperatures of reaction were described in the previous section). The DSC analysis showed an endothermic peak close to the transition of solid to liquid phase confirming the data obtained from thermodynamic calculations. Figures 8–10 demonstrate the evolution of the liquid fraction in function of the temperature. Figure 8 shows the effect of Al₂O₃ content on the liquid fraction of the deposits.

Typically, the side ledge at the bottom of the cell is undersaturated and its melting temperature is extremely sensitive to the [Al₂O₃]. In undersaturated bath, the alumina decreases the melting temperature of Na₃AlF_{6(ss)}. According to thermodynamic calculations, complete melting occurs at 970 °C when [Al₂O₃] = 1 % while it occurs at 944 °C when [Al₂O₃] = 5 %. The side ledge and ledge toe are formed when the local temperature is lower than the temperature of the solidification of Na₃AlF_{6(ss)} (933 °C with CR = 2.2, CaF_{2,eq} = 5 % and Al₂O₃ = 10 %). The side ledge behaves like solid deposits during the operation of the electrolysis cell, as it is attached on the sidewall during the operation. However, liquid bath exists at

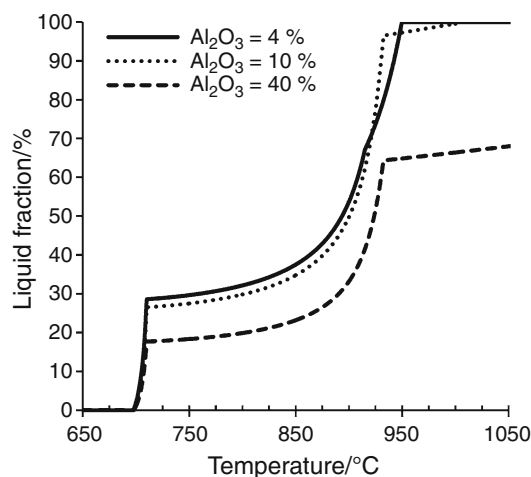


Fig. 8 Liquid bath fraction, with CR = 2.2 and CaF_{2,eq} = 5 %, depending on the Al₂O₃ content

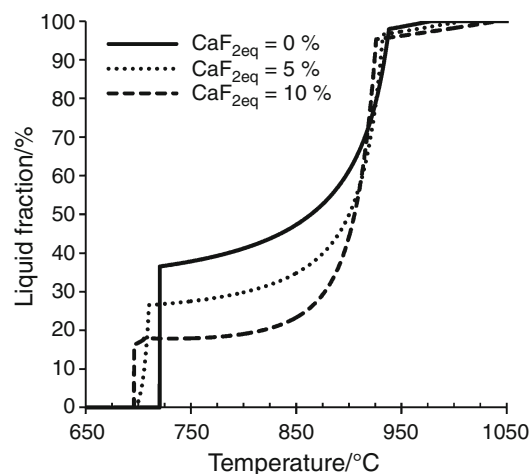


Fig. 9 Liquid bath fraction, with CR = 2.2 and Al₂O₃ = 10 %, depending on CaF_{2,eq}

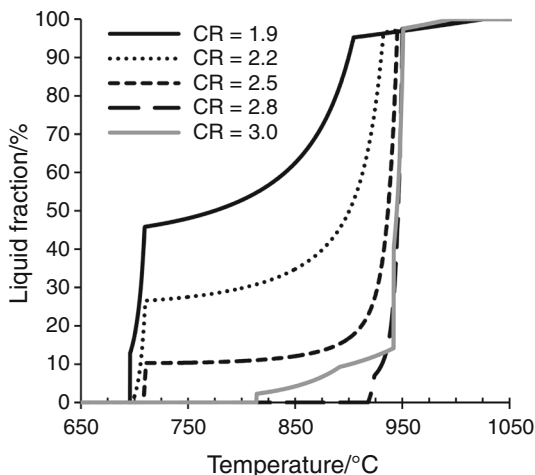


Fig. 10 Liquid bath fraction, with CaF_{2,eq} = 5 % and Al₂O₃ = 10 %, depending on CR

temperatures higher than 698 °C in acid bath and a fraction of the side ledge is composed by liquid. The liquid bath may be “trapped” between the $\text{Na}_3\text{AlF}_6(\text{ss})$ crystals. Similar observations were made by Fallah-Mehrijardi et al. with the $\text{NaF-CaF}_2\text{-AlF}_3$ system [16]. There is a temperature gradient due to the heat losses at the sidewall and the liquid fraction varies depending on the local temperature.

The ledge toe near the sidewall has a similar composition to the side ledge facing the metal and its $[\text{Al}_2\text{O}_3]$ increases farther from the sidewall. Thus, the extremity of the ledge toe can be described as a bath supersaturated in Al_2O_3 . The alumina content decreases the liquid fraction according to the low solubility of alumina. The ledge toe ($[\text{Al}_2\text{O}_3] = 10\text{--}40\%$) and the sludge ($[\text{Al}_2\text{O}_3] = 40\%$) on the cathode block surface are all in contact with liquid aluminum. The sludge behaves like a mixture of solid alumina in liquid electrolytic bath if its temperature is higher than 933 °C. It will behave like solid crust if the heat loss from the bottom of the cell is sufficient to decrease its temperature under 933 °C (with $\text{CR} = 2.2$ and $\text{CaF}_{2\text{eq}} = 5\%$).

As it can be seen in Fig. 9, $[\text{CaF}_2]$ in deposits also has an impact on the solidification of the deposits. High $[\text{CaF}_2]$ decreases the solubility of Al_2O_3 in bath and it decreases the liquid bath fraction at temperatures higher than 720 °C. The melting of the bath begins at lower temperature with higher $[\text{CaF}_2]$. The CaF_2 affects the formation of side ledge and ledge toe according to its impact on the melting temperature of $\text{Na}_3\text{AlF}_6(\text{ss})$.

Figure 10 shows the impact of the CR on the liquid fraction. The NaF/AlF_3 content in the bath has a major impact on the formation of side ledge and ledge toe. The solidification of $\text{Na}_3\text{AlF}_6(\text{ss})$ begins at 905 °C ($\text{CR} = 1.9$), 933 °C ($\text{CR} = 2.2$), 946 °C ($\text{CR} = 2.5$), and 951 °C ($\text{CR} = 2.8$). The risk of the formation of solid deposits on the cathode is higher with lower acidity. Furthermore, the melting of $\text{Na}_3\text{AlF}_6(\text{ss})$ occurs within a short temperature interval at CR between 2.8 and 3.0. The bath of $\text{CR} = 3.0$ began to melt at a lower temperature than the bath of $\text{CR} = 2.8$ as explained in the description of the CR phase diagram (Fig. 7).

According to this analysis, the ledge toe contains a major fraction of liquid phase. The local temperature of this deposit can be lower than 933 °C [25]. This deposit has a CR between 2.2 and 2.8 and has a $[\text{CaF}_{2\text{eq}}] \sim 5\%$ (Table 1). Thus, the liquid phase in the ledge toe is due to the content in $\text{Na}_5\text{Al}_3\text{F}_{14}$, $\text{Na}_2\text{Ca}_3\text{Al}_2\text{F}_{14}$, and NaCaAlF_6 . The ledge toe interacts with the bath film found between the ledge and the aluminum pad. The liquid bath into the ledge toe and the side ledge facing the metal may diffuse toward the bath film.

Thermogravimetry and differential thermal analysis

Thermogravimetric analyses were completed in order to evaluate the mass losses of samples during the

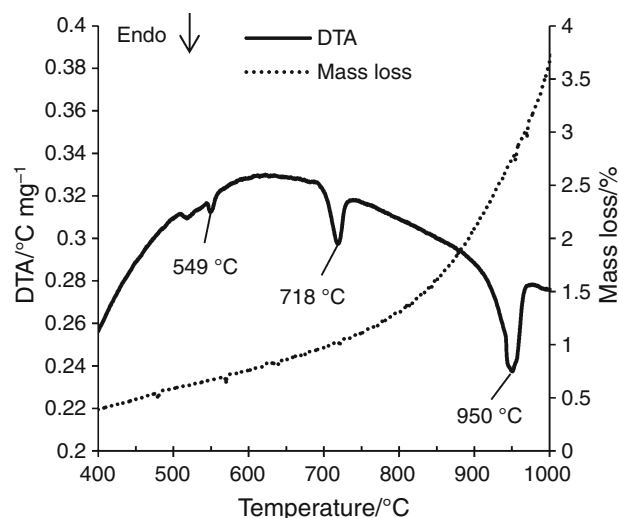


Fig. 11 TG/DTA analysis of a bath with $\text{CR} = 2.2$, $\text{CaF}_{2\text{eq}} = 5\%$ and $\text{Al}_2\text{O}_3 = 10\%$

measurement of the endothermic peaks. They were conducted with open crucible and under argon atmosphere. Figure 11 shows the temperature difference between the sample and the reference material (DTA) and the mass losses as a function of the furnace temperature.

This test was performed with a bath of $\text{CR} = 2.2$, $\text{CaF}_{2\text{eq}} = 5\%$ and $\text{Al}_2\text{O}_3 = 10\%$. The rate of mass losses increased above 718 °C according to thermogravimetric analysis. At 1,000 °C there was a mass loss of 3.7 % with the bath of $\text{CR} = 2.2$. The same test was conducted with a bath of $\text{CR} = 1.9$ with similar results. The evaporation of the volatile phase in the sample affects the results of the DSC experiments. According to the literature, the metastable phase NaAlF_4 can be found from quenched vapor and is the dominant gaseous species in Na_3AlF_6 melt [26, 27]. Consequently, the CR will increase during the DSC or DTA experiments due to the evaporation of acidic phase (NaAlF_4). The cover used in the DSC experiments helped to reduce the mass loss.

The peak at 718 °C was not detected in the TG/DTA analysis of Na_3AlF_6 (Fig. 12). In this case, thermogravimetric analysis demonstrated an increasing rate of mass loss near from 880 °C. This rate increased significantly after the melting of the Na_3AlF_6 at 1,005 °C. The mass losses in the sample of Na_3AlF_6 were 1.1 % at 1,000 °C. The mass losses increased quickly at temperature higher than 1,000 °C and it reached 5 % at 1,100 °C.

Industrial implications of the results

An excessive formation of ledge toe or an important sludge accumulation under the aluminum pad reduces the contact surface between the aluminum and the cathode block, a situation leading to an increased voltage drop and higher

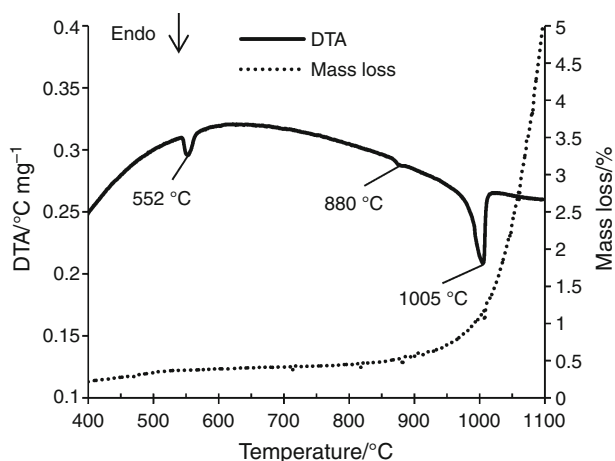


Fig. 12 TG/DTA analysis of Na_3AlF_6

Table 3 Summary of the main phase transitions in the deposits

Type of deposits	CR	Al_2O_3 / %	T_{solidus} / °C	$T_{\text{Na}_3\text{AlF}_6}$ / °C	$T_{\text{Al}_2\text{O}_3}$ / °C
Side ledge or undersaturated ledge toe	2.2	4	698	950	915
	2.5	4	708	965	938
	2.8	4	918	971	947
Sludge or supersaturated ledge toe	2.2	40	698	933	>1,100
	2.5	40	708	946	>1,100
	2.8	40	918	951	>1,100
	3.0	40	814*	951	>1,100

energy consumption. The formation of deposits on the cathode surface should be controlled in order to minimize the electric current restriction. An excessive expansion of the ledge toe on the cathode surface also modifies the current path and generates horizontal current which disturbs the process by increasing the motion of the metal. The chemical compositions of the electrolytic bath could be controlled in order to minimize the formation of deposits. Table 3 summarizes the temperature of the main phase transitions in the side ledge, ledge toe, and sludge of typical chemical composition. The $[\text{CaF}_{2\text{eq}}]$ was kept at 5 % for the thermodynamic calculations.

T_{solidus} is the temperature when the bath completely freezes. $T_{\text{Na}_3\text{AlF}_6}$ is the melting temperature of $\text{Na}_3\text{AlF}_6(\text{ss})$. $T_{\text{Al}_2\text{O}_3}$ is the temperature corresponding to the saturation of Al_2O_3 in bath. The solidus at 814 °C (CR = 3.0, $[\text{Al}_2\text{O}_3] = 40\%$) was not detected in the DSC analysis. The chemical compositions were selected in order to globally reproduce the data from the previous studies of the deposits in industrial cells [10–13, 17]. The temperature range in the side ledge is between the process temperature ($\sim 960\text{ °C}$) and below 700 °C according to simulation results [1]. The temperature of the ledge toe is close to the

process temperature, but lower than the melting temperature of $\text{Na}_3\text{AlF}_6(\text{ss})$ [25]. The temperature of the sludge is similar to the process temperature. The temperature range in the deposits depends on the heat loss by the sidewall and the bottom of the cell.

The melting temperature of $\text{Na}_3\text{AlF}_6(\text{ss})$ in ledge toe decreases when the $[\text{CaF}_2]$ and $[\text{AlF}_3]$ increase, which is a favorable situation if one wants to reduce the amount of ledge toe and bottom freeze. However, higher $[\text{CaF}_2]$ and $[\text{AlF}_3]$ in the bath may also lead to the melting of the side ledge boundary facing the bulk bath. The $[\text{CaF}_2]$ also slightly decreases the melting temperature of $\text{Na}_5\text{Al}_3\text{F}_{14}$. Other additives like LiF, MgF_2 , or KF will also decrease the melting temperature of compounds inside the deposits [4]. The ledge toe near the sidewall has a chemical composition similar to the side ledge facing the metal. Moreover, the chemistry of the side ledge at the bottom of the cell may be similar to the chemistry of the bath [17]. However, the side ledge facing the bath is generally more neutral. A side ledge formed at equilibrium conditions has a composition close to pure Na_3AlF_6 [15]. The extremity of the ledge toe farther from the sidewall and the sludge are more supersaturated in alumina and less acidic than the bath above the metal. For such compounds, one finds a higher melting temperature of $\text{Na}_3\text{AlF}_6(\text{ss})$ based on thermodynamic calculations and DSC analysis (Table 3). The liquidus of such deposits is also higher due to the high content of Al_2O_3 . An acidic side ledge (CR between 2.2 and 2.5) freezes completely at a temperature around 700 °C depending on $[\text{AlF}_3]$ and $[\text{CaF}_2]$. The liquid fraction in the ledge toe close to the sidewall varies from 95 to 25 % at a temperature range from 933 to 710 °C (CR = 2.2, $\text{CaF}_{2\text{eq}} = 5\%$ and $\text{Al}_2\text{O}_3 = 10\%$). Deposits with such chemical composition completely freeze at 698 °C and completely melt at $1,009\text{ °C}$ (933 °C without considering the Al_2O_3 dissolution). The temperature of the sludge and the extremity of the ledge toe is very close to the temperature of solidification of $\text{Na}_3\text{AlF}_6(\text{ss})$. These deposits will be composed by solid Al_2O_3 in liquid bath at higher temperature than $T_{\text{Na}_3\text{AlF}_6}$. At lower temperature, they will be mostly solid with acidic liquid species “trapped” into the Na_3AlF_6 dendrites and $\alpha\text{-Al}_2\text{O}_3$ platelets.

Conclusions

The DSC experiments confirmed the temperature of $\alpha\text{-Na}_3\text{AlF}_6$ to $\beta\text{-Na}_3\text{AlF}_6$ transition, the melting of $\text{Na}_5\text{Al}_3\text{F}_{14}$ and the melting of $\text{Na}_3\text{AlF}_6(\text{ss})$ as calculated by the thermodynamic equilibrium. The first heating of the synthetic bath shows a similar conversion of $\alpha\text{-Na}_3\text{AlF}_6$ to $\beta\text{-Na}_3\text{AlF}_6$ than pure Na_3AlF_6 (at 563 °C according to thermodynamic calculations). This temperature of conversion

decreased to 526 °C when NaCaAlF₆ is dissolved in the Na₃AlF_{6(ss)}. The use of closed graphite crucibles helped to obtain a better base line and to achieve an improved repeatability of results. The thermodynamic equilibrium calculations were used to produce phase diagrams at various [Al₂O₃], [CaF₂], and CR. The solidification and melting of the bath in the side ledge, ledge toe, and sludge are highly influenced by the [AlF₃] and [CaF₂]. The CR of the bath and the [CaF₂] will affect the behavior of these materials during the process of aluminum production. The first liquid phase in the deposits appears around 700 °C depending on the [AlF₃] and [CaF₂]. The liquid fraction in the deposits is due to the presence of Na₅Al₃F₁₄, Na₂Ca₃Al₂F₁₄, and NaCaAlF₆. Modeling studies of the freeze formation in an electrolysis cell may have to be adjusted by considering the liquid fraction as a function of the chemical composition. The sludge close to the aluminum mainly consists of solid alumina in liquid electrolytic bath with a low acidity. The temperature at the bottom of the electrolysis cell must be kept at temperature higher than 951 °C in order to avoid the risk of freezing of low acidity sludge or to reduce the expansion of the ledge toe (CR of 2.8).

Acknowledgements The authors are grateful to the employees of the “Centre de Caractérisation des Matériaux” for their help with the various characterization devices and to the chemist, Mr. Carl St-Louis, who helped to elaborate the DSC method. The authors also thank Alireza Hekmat and Lynne Davies for manuscript revision and correction. This work is financed and supported by Rio Tinto Alcan, “Conseil de Recherches en Sciences Naturelles et en Génie du Canada” (CRSNG) and “Fonds de Recherche du Québec-Nature et Technologies” (FRQNT).

References

- Sørli M, Øye HA. Cathodes in aluminium electrolysis. 3rd ed. Düsseldorf: Aluminium-Verlag; 2010.
- Chartrand P, Pelton AD. A predictive thermodynamic model for the Al-NaF-AlF₃-CaF₂-Al₂O₃ system. *Light Met* 2002, Proc Int Symp. 2002;245–52.
- Apisarov A, Dedyukhin A, Nikolaeva E, Tinghaev P, Tkacheva O, Redkin A, Zaikov Y. Liquidus temperatures of cryolite melts with low cryolite ratio. *Metall Mater Trans B*. 2011;42:236–42.
- Solheim A, Rolseth S, Skybakmoen E, Støen L, Sterten Å, Støre T. Liquidus temperatures for primary crystallization of cryolite in molten salt systems of interest for aluminum electrolysis. *Metall Mater Trans B*. 1996;27:739–44.
- Tissot P. DTA determination of liquidus temperatures and Al₂O₃ and AlF₃ content in cryolitic melts. *Thermochim Acta*. 1994;234:245–54.
- Peterson RD, Tabereaux AT. Liquidus curves for the cryolite—AlF₃—CaF₂—Al₂O₃ system in aluminum cell electrolytes. *Light Met* 1987, Proc Int Symp. 1987;383–8.
- Danielik V, Gabčová J. Phase diagram of the system NaF—KF—AlF₃. *J Therm Anal Calorim*. 2004;76:763–73.
- Skybakmoen E, Solheim A, Sterten Å. Alumina solubility in molten salt systems of interest for aluminum electrolysis and related phase diagram data. *Metall Mater Trans B*. 1997;28:81–6.
- Coursol P, Dufour G, Côté J, Chartrand P, Mackey P. Application of thermodynamic models for better understanding and optimizing the Hall-Heroult process. *JOM*. 2012;64:1326–33.
- Allard F, Coulombe MA, Soucy G, Rivoaland L. Cartography and chemical composition of the different deposits in the Hall-Heroult process. *Light Met* 2014, Proc Int Symp. 2014;1233–8.
- Thonstad J, Ronning S, Entner P. Formation of bottom crusts in aluminum pots—a laboratory study. *Light Met* 1982, Proc Int Symp. 1982;485–97.
- Keller R. Alumina dissolution and sludge formation revisited. *Light Met* 2005, Proc Int Symp. 2005;147–150.
- Geay PY, Welch BJ, Homs P. Sludge in operating aluminium smelting cells. *Light Met* 2001, Proc Int Symp. 2001;2:541–7.
- Solheim A, Stoen L. On the composition of solid deposits frozen out from cryolitic melts. *Light Met* 1997, Proc Int Symp. 1997;325–32.
- Solheim A. Some aspects of heat transfer between bath and sideledge in aluminium reduction cells. *Light Met* 2011, Proc Int Symp. 2011;381–6.
- Fallah-Mehrjardi A, Hayes PC, Jak E. Investigation of freezeline in aluminum production cells. *Metall Mater Trans B*. 2014;. doi:10.1007/s11663-014-0078-z.
- Allard F, Soucy G, Rivoaland L. Formation of deposits on the cathode surface of aluminum electrolysis cells. *Metall Mater Trans B*. 2014;. doi:10.1007/s11663-014-0118-8.
- Lukas K, LeMaire PK. Differential scanning calorimetry: fundamental overview. *Resonance*. 2009;14:807–17.
- Haines PJ. Thermal methods of analysis: principles, applications and problems. 1st ed. London: Chapman & Hall; 1995.
- Cuesta D, Gómez MA, Porteiro J, Febrero L, Granada E, Arce E. CFD analysis of a TG–DSC apparatus. *J Therm Anal Calorim*. 2014;. doi:10.1007/s10973-014-3734-2.
- Zaitseva JN, Yakimov IS, Kirik SD. Thermal transformation of quaternary compounds in NaF–CaF₂–AlF₃ system. *J Solid State Chem*. 2009;182:2246–51.
- Feret FR. Breakthrough in analysis of electrolytic bath using Rietveld-XRD method. *Light Met* 2008, Proc Int Symp. 2008;343–6.
- Craig DF, Brown JJ. Phase equilibria in the system CaF₂–AlF₃–Na₃AlF₆ and part of the system CaF₂–AlF₃–Na₃AlF₆–Al₂O₃. *J Am Ceram Soc*. 1980;63:254–61.
- Holm JL. The phase diagram of the system Na₃AlF₆–CaF₂, and the constitution of the melt in the system. *Acta Chem Scand*. 1968;22:1004–12.
- Taylor MP, Liu X, Fraser KJ, Welch BJ. Dynamics and performance of reduction cell electrolytes. *Light Met* 1990, Proc Int Symp. 1990;259–66.
- Howard EH. Some physical and chemical properties of a new sodium aluminum fluoride. *J Am Chem Soc*. 1954;76:2041–2.
- Kvande H. Vapour-phase studies of NaF–AlF₃ melts. 1. The AlF₃–rich part. *High Temp High Press*. 1983;15:51–62.